POLITECNICO DI TORINO
Repository ISTITUZIONALE

Enhancing the pressure and force ranges of variable stiffness Soft Pneumatic Sensing Chambers via deformable reservoirs

Original
Enhancing the pressure and force ranges of variable stiffness Soft Pneumatic Sensing Chambers via deformable reservoirs / Duretto, S., Selvaggi, E., Colucci, G., Quaglia, G.. - ELETTRONICO. - 9:(2026), pp. 22-29. (The 9th Jc-IFToMM International Symposium (in conjunction with The 32nd Jc-IFToMM Symposium on Theory of Machines and Mechanisms) Tokyo (JPN) June 11, 2026 - June 12, 2026) [10.57272/jciftomm.9.0_22].

Availability:
This version is available at: 11583/3016553 since: 2026-10-13T08:54:28Z

Publisher:
Japanese Council of IFToMM

Published
DOI:10.57272/jciftomm.9.0_22

Terms of use:

This article is made available under terms and conditions as specified in the corresponding bibliographic description in the repository

Publisher copyright

(Article begins on next page)

28 November 2026

Proceedings of the 9th Jc-IFToMM International Symposium (2026)
The 32nd Jc-IFToMM Symposium on Theory of Machines and Mechanisms
11-12 June 2026

Enhancing the Pressure and Force Ranges of Variable Stiffness Soft Pneumatic Sensing Chambers via Deformable Reservoirs

Simone Duretto, Edoardo Selvaggi, Giovanni Colucci, Giuseppe Quaglia
Department of Mechanical and Aerospace Engineering, Politecnico di Torino, Italy,
{simone.duretto, giovanni_colucci, giuseppe.quaglia}@polito.it
edoardo.selvaggi@studenti.polito.it

Abstract
Soft Pneumatic Sensing Chambers (SPSCs) have the potential to significantly enhance robotic manipulation through their compliance, tactile sensing capabilities, and tunable stiffness. This study expands the pressure and force ranges of an SPSC system with discretely tunable stiffness by integrating a deformable reservoir. Results demonstrate that pressure and force ranges increase by 4.1% and 49.7%, respectively. Then, the transition between the low and high stiffness configurations is assessed. On average, achieving a 5 N force difference requires 1.0 mm of additional compression, while around the transition point the pressure sensitivity increases from 0.4 to 4.8 kPa/mm.

Keywords: Soft Sensor, Tactile Sensing, Compliant Grasping, Controlled Stiffness

1. Introduction

Soft Pneumatic Sensing Chambers (SPSCs) are deformable, airtight, and monolithic sensors characterized by inherit compliance, repeatability, and negligible hysteresis [1]. They are typically manufactured using accessible 3D-printing techniques such as Fused Deposition Modeling (FDM) and Stereolithography (SLA), or by silicone casting.

SPSCs are mainly used in applications requiring a safe and compliant interaction with the environment, including compliant grasping and Human-Machine Interfaces (HMI). Specifically, in the field of robotic manipulation, it is established that the interposition of a soft, compliant element between the gripper and the grasped object considerably reduces control complexity [2, 3]. Moreover, it is proven that controlled stiffness plays a fundamental role in versatile robotic grasping [4], by extending the range of objects that a gripper can successfully grasp. Finally, while compliance effectively manages positioning uncertainties, it presents inherent physical limits in force transmission and stability. Therefore, tactile sensing is fundamental to ensure robust grasping performance [5].

Motivated by this, the authors have previously investigated the use of an SPSC-based system for compliant grasping and tactile sensing, with stiffness discretely tunable between two configurations (i.e., low and high stiffness) [6, 7]. In this work, a new pneumatic control system featuring a deformable reservoir is introduced and tested, in order to enhance the achievable ranges of pressure and force. Moreover, the transition between the low and high stiffness configurations is assessed.



(c) 2026 The Authors. This is an open access article under the terms of the Creative Commons Attribution License.
(https://creativecommons.org/licenses/by/4.0/)

2. Functional Design and Modeling

The sensing system is made of a soft bladder *B* which is connected to an auxiliary pneumatic system, as depicted in Fig. 1(a). The auxiliary system comprises a pressure transducer *PT* and a solenoid valve *D*, which is used to either open or close the connection between the bladder and a deformable reservoir *R*. Therefore, the system can switch between two discrete stiffness levels (either low or high stiffness) by controlling, through the solenoid valve *D*, the volume of air undergoing deformation. With respect to the previous version of the system [6, 7], the rigid reservoir has been replaced with a deformable one, and the new design has been further simplified by removing the check valve. As it will be illustrated in Section 3.2, with respect to the original design, these choices allow to further separate the pressure and force curves between the low and high stiffness configurations, while reducing the number of components and the volume required to allocate them. As a compromise, the possibility of changing the minimum stiffness level by preloading the system with compressed air was abandoned, giving priority to the enhanced separation of the low and high stiffness levels.

2.1 Deformable Reservoir Modeling

The deformable reservoir consists of a flat, circular membrane which is clamped between two rigid elements to define a closed volume, as detailed in Fig. 1(d). The circular membrane is made of a soft material, so that it can easily deform as the pressure in the system increases. It is critical that the material and geometric parameters of the membrane (e.g., thickness) are carefully selected not to introduce excessive structural stiffness in the system. Indeed, significant stresses are induced in the deformable diaphragm as it stretches, which turns into additional perceived stiffness in the system. However, in this instance the flat membrane design was preferred to rolling diaphragms for the relatively low pressures involved, and for the ease of fabrication.

The approximate pressure–volume curve of the deformable reservoir can be derived as proposed by Yuan et al. [8], by assuming that:

1. The membrane has a nominal radius of R_0 and a nominal thickness of t_0, as shown at the top of Fig. 1(c).
2. To mount the membrane on the rigid base, it is required to equi-biaxially pre-stretch the membrane with a stretching ratio $\lambda_0 \geq 1$, after which its radius and thickness become $R_1 = \lambda_0 R_0$ and $t_1 = \Lambda_0 t_0$, respectively, with $\Lambda_0 = 1/\lambda_0^2$ (deriving from the incompressibility condition).
3. The bending stiffness of the membrane is neglected, i.e., there are only in-plane tensile stresses.
4. The deformed membrane is shaped as a spherical cap, with radius R, height H and volume V, as depicted at the bottom of Fig. 1(c).

Under these assumptions, the pressure–volume curve is given as follows:

$$p(V) = \frac{2t_0}{R_0}\Lambda_0^{\frac{3}{2}}\cos^2\left(\frac{\vartheta(V)}{2}\right)\sin\vartheta(V) \cdot \sigma\big(\Lambda(V)\big) \tag{1}$$

where p is the gauge pressure in the system, V is the volume of the spherical cap, while $\Lambda(V)$, $\vartheta(V)$ and V_0 are defined as follows:

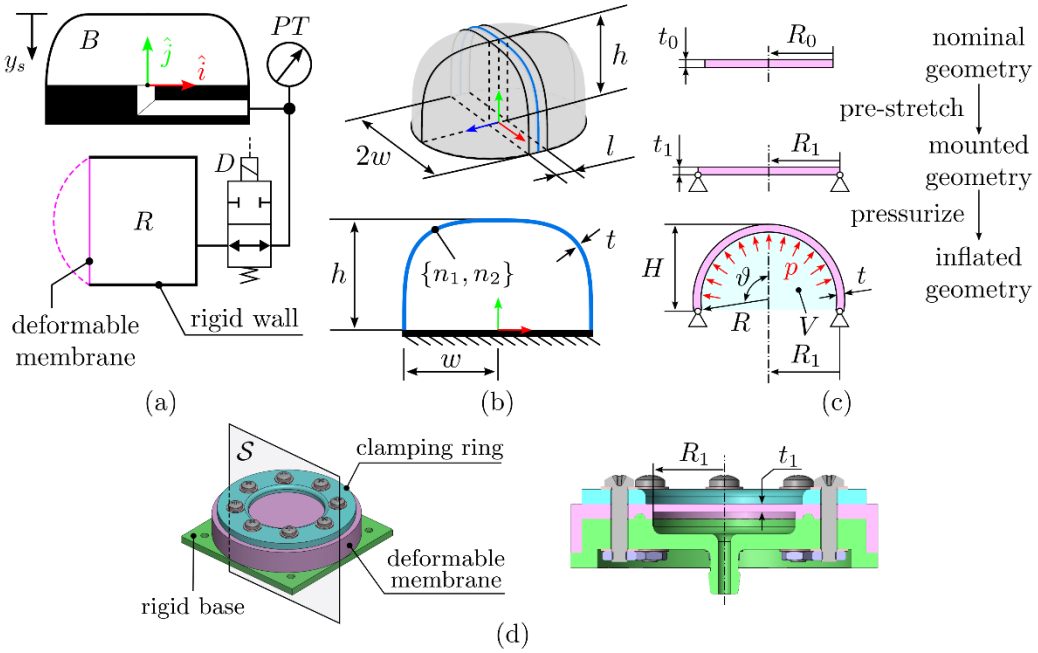

Fig. 1 – (a) SPSC system with a deformable reservoir. The pink solid line represents the initial configuration, while the dashed line the deformed one. (b) Geometric definition of the SPSC unit and its relevant parameters. (c) Nominal, mounted, and inflated geometry of the deformable membrane, with relevant parameters. Mounting the membrane on the rigid base requires to pre-stretch the membrane to increase its radius from R_0 to R_1. (d) Axonometric view of the deformable reservoir and section view through plane $\mathcal{S}$.

$$\Lambda(V) = \left(\frac{\sin\left(\frac{\vartheta(V)}{2}\right)}{\frac{\vartheta(V)}{2}} \right)^2 \cdot \cos^2\left(\frac{\vartheta(V)}{2}\right) \tag{2}$$

$$\vartheta(V) = 2\text{atan}\left(\sqrt[3]{\sqrt{1+\left(2\Lambda_0^{\frac{3}{2}}\frac{V}{V_0}\right)^2} + 2\Lambda_0^{\frac{3}{2}}\frac{V}{V_0}} - \sqrt[3]{\sqrt{1+\left(2\Lambda_0^{\frac{3}{2}}\frac{V}{V_0}\right)^2} - 2\Lambda_0^{\frac{3}{2}}\frac{V}{V_0}} \right) \tag{3}$$

$$V_0 = \frac{2}{3}\pi R_0^3 \tag{4}$$

The function $\sigma(\Lambda)$ in Eq. (1) represents the expression of the equi-biaxial tension, which depends on the hyperelastic material model selected. Assuming a 3rd order Yeoh hyperelastic model, then:

$$\sigma(\Lambda) = 2\left(\frac{1}{\Lambda_0\Lambda} - \Lambda_0^2\Lambda^2\right)\left[C_1 + 2C_2\left(\frac{2}{\Lambda_0\Lambda} + \Lambda_0^2\Lambda^2 - 3\right) + 3C_3\left(\frac{2}{\Lambda_0\Lambda} + \Lambda_0^2\Lambda^2 - 3\right)^2\right] \quad (5)$$

Figure 2 presents a comparison of pressure–volume curves for different combinations of materials, thicknesses, and pre-stretching ratios, with a fixed in-place radius of the membrane of R_1 = 10.5 mm. Two materials have been considered, namely Elastic 50A (Formlabs) and Ecoflex 00-50 (Smooth-On Inc.), which are modelled with a Yeoh 3rd order model. The material coefficients for Elastic 50A have been retrieved from [9] (C_1 = 1.39e-2 MPa, C_2 = 1.11e-4 MPa, C_3 = -8.76e-8 MPa), while the coefficients for Ecoflex 00-50 have been independently derived from the static test data given in [10] (C_1 = 5.15e-1 MPa, C_2 = 0 MPa, C_3 = 3.37e-3 MPa).

The analysis shows that Elastic 50A is too stiff for this application, even at the smallest thickness considered. Reducing the thickness further could be beneficial, but below a certain threshold the manufacturing of the membrane through Stereolithography (SLA) becomes impractical. On the other hand, Ecoflex 00-50 generally presents a satisfactory behavior for all combinations of parameters. It is observed that a moderate pre-stretching of 10% can help reduce the wrinkling of the soft membrane as it is clamped between the rigid parts of the reservoir. However, from a practical point of view, wrinkling does not significantly affect operation, thus a pre-stretching ratio of 0% will be used in the following.

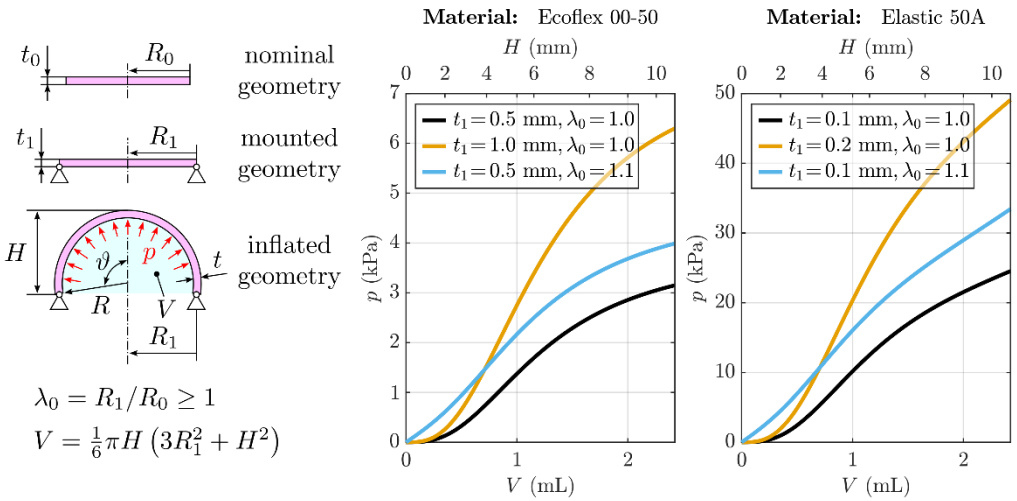

Fig. 2 – Parametric analysis of the pressure–volume curve obtained by combining different materials, thicknesses and pre-stretching ratios. In this instance, R_1 is fixed at 10.5 mm.

3. Experimental Characterization

3.1 Characterization of the Deformable Reservoir

A deformable reservoir with a flat diaphragm, with R_0 = 10.5 mm, t_0 = 0.5 m, λ_0 = 1, made from Ecoflex 00-50, was characterized to compare the expected and experimental pressure–volume curves. The reservoir was connected to a pressure source, and the pressure was gradually increased. The pressure inside the reservoir was measured using an absolute pressure sensor (NXP

Semiconductors MPXH6300AC6T1, F.S. 304 kPa, precision 1.5%) connected to a NI USB-6002 (National Instruments Corp.). The deformed profile of the membrane was recorded via a camera. Then, during post-processing, the profile of the membrane was extracted through image processing.

The results of this analysis are given in Fig. 3, where the shape of the inflated membrane and the circular arcs that approximate the deformed profile are represented, together with the pressure–volume curve. For convenience, for each pressure the height of the highest point of the inflated membrane has been reported as well. As shown, there is a fairly good accordance between the estimated and the experimental pressure–volume curves. It must be noted that the initial portion of the experimental curve is affected by the wrinkling of the membrane due to the clamping force, which results in the membrane not to be initially flat, but already deformed with an initial height of the top point greater than zero. Finally, in the last portion the experimental curve starts deviating significantly from the estimated one, which is likely due to the activation of edge stiffness.

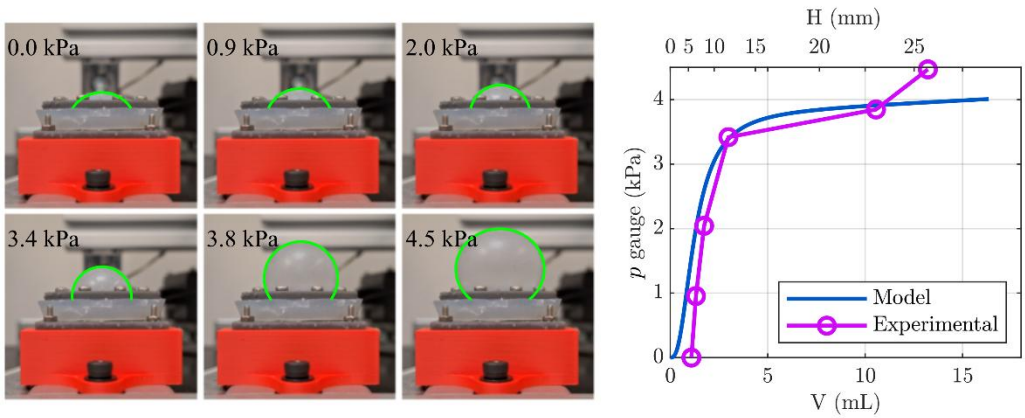

Fig. 3 – Experimental characterization of a deformable reservoir with R_0 = 10.5 mm, t_0 = 0.5 mm and λ_0 = 1, and comparison between the experimental and estimated pressure–volume curves.

3.2 Characterization of the SPSC System

The SPSC system equipped with the deformable reservoir has been tested against the version with the rigid reservoir, which in this instance has a volume of 26 cm^3. For this analysis, an SPSC of Type A is considered, since it is the most suitable for tactile sensing applications, as discussed in [11].

For convenience, the definition of Type A SPSC is briefly provided. The SPSC is defined by thickening by a quantity t and extruding by a quantity l from the mid-plane a *super-ellipse* curve, as shown in Fig. 1(b); then, the SPSC is closed at the two lateral edges by extruded revolutions. Specifically, the explicit equation of the super-ellipse for $x > 0$ is the following:

$$y = h \cdot \left[1 - \left(\frac{x}{w}\right)^{n_1}\right]^{1/n_2} \tag{6}$$

with w and h representing, respectively, the encumbrance at the fixed edge and the height of the cross section, while $\{n_1, n_2\}$ are used as control parameters to change the shape of the cross section

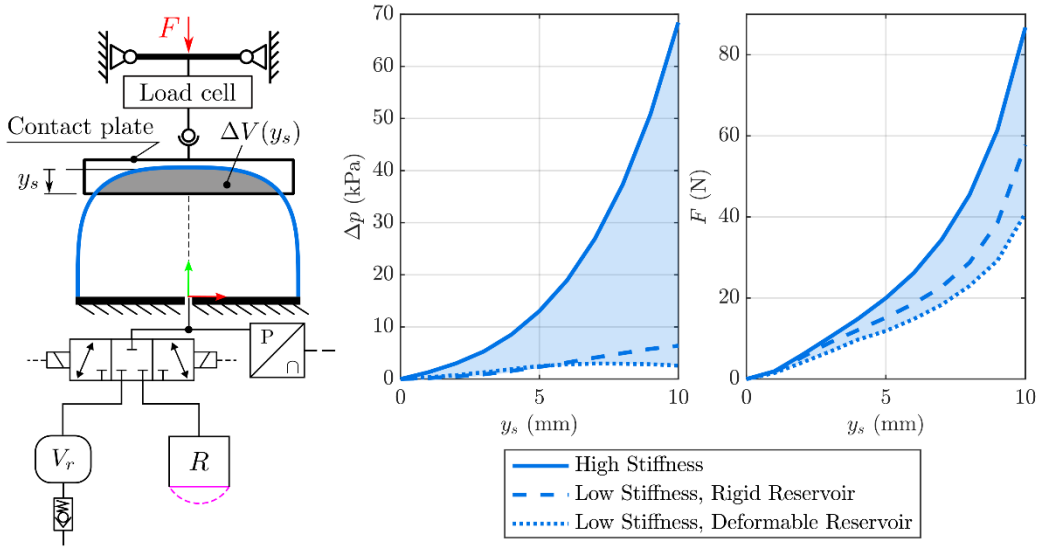

Fig. 4 – Comparison of the static pressures and forces obtained by connecting the SPSC unit either to a rigid or a deformable reservoir. The performance with the SPSC unit isolated is reported as well.

(see Fig. 1(b)). The Type A SPSC considered has w = 11 mm, h = 13 mm, l = 3 mm, t = 1 mm, n_1 = 3, n_2 = 4, and it is made from Filaflex TPU 60A PRO (Recreus Industries S.L.).

The system was tested by connecting the Type A SPSC either to a rigid reservoir with an internal volume of 26 cm^3 or a deformable reservoir with the same parameters defined in Section 3.1. A 3 ways – 2 positions solenoid valve (model FA0520E, supplied by Adafruit Industries), modified to serve as a 2/2 valve, was used to connect the SPSC to the auxiliary reservoir. Pressure inside the system was measured by an absolute pressure sensor (NXP Semiconductors MPXH6300AC6T1, F.S. 304 kPa, precision 1.5%). A rigid plate, constrained by a linear guide to translate along the vertical direction only, uniformly squeezes the bladder. The pressing force was measured by a load cell (LCM Systems DCE-500N, F.S. 500 N, non-linearity ±0.25%), and a NI USB-6002 (National Instruments Corp.) was used to acquire all analog signals.

Figure 4 shows the comparison between the static performance of the two systems in the low stiffness configuration. The performance in the high stiffness configuration has been reported as well. The results show that the achievable ranges of pressure and force, defined as the area enveloped by the curves corresponding to the low and high stiffness conditions, increases by 4.1% and 49.7%, respectively. It should be noted that, although a comparable improvement could be obtained by increasing the volume of the rigid reservoir, that solution is not always feasible, especially when there are tight space and weight constraints, as in the case when the sensing system is mounted on the end-effector of a manipulator.

It is also of interest to study the transition between the low and high stiffness configurations while the SPSC unit is being pressed. In fact, when the proposed SPSC system is used for compliant grasping and tactile sensing, the object should first be approached in a low stiffness mode to achieve a gentle grasp. Then, based on the inferred object stiffness (the greater the object stiffness, the more

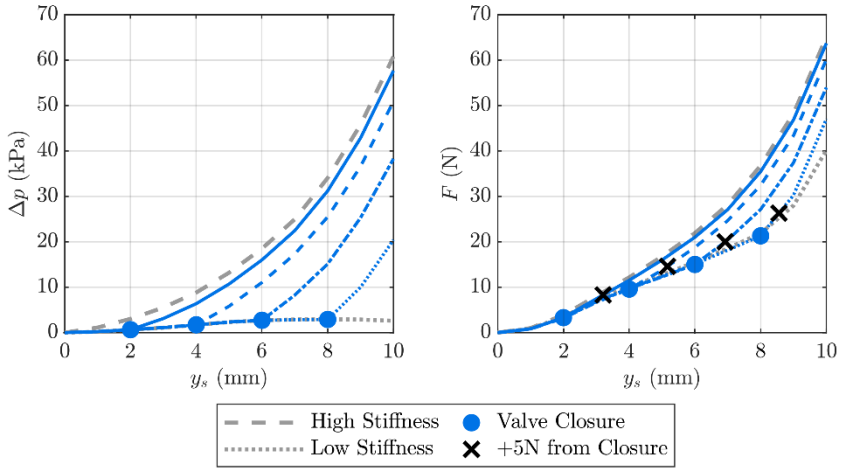

Fig. 5 – Analysis of the transition from low to high stiffness configuration at different contact depths y_s.

the pressure increase for a given finger closure), the system switches to the high stiffness mode, and the fingers are further closed (more if the object is rigid) to stabilize the grasp [5]. For this reason, it is required to evaluate if the system can produce enough force to stabilize the grasp without requiring too much additional finger closure, which can damage the grasped object.

Figure 5 reports the experimental results. The transition from low to high stiffness has been repeated for contact depths y_s in the range 0÷10 mm, with steps of 2 mm. Specifically, it is found that, on average, to achieve at least 5 N of difference in force after the transition, the SPSC needs to be further pressed by 1.0 mm, with a maximum of 1.2 mm when the transition happens at 2 mm and minimum of 0.6 mm when it occurs at 8 mm. The mean pressure sensitivity was found to increase from 0.4 to 4.8 kPa/mm around the transition points.

4. Conclusions

This study focused on the development and testing of an auxiliary pneumatic system to enhance the static performance of an SPSC unit for robotic manipulators. The use of a deformable reservoir proved to increase the range of achievable pressures and forces as compared to a rigid reservoir. Specifically, the range of pressures increased by 4.1%, while the range of forces increased by 49.7%. When transitioning from low to high stiffness configurations, on average, contact depth had to be increased by 1.0 mm to increase the force by 5 N, while the pressure sensitivity increased from 0.4 to 4.8 kPa/mm around the transition points.

While these results demonstrated the effectiveness of the proposed solution for the application in robotic manipulation, future work will focus on further enhancing the sensing system's performance by modifying the deformable reservoir design. By adding a closed chamber atop the reservoir to act as a pneumatic spring, the SPSC system can be filled with an incompressible fluid and pre-charged. This configuration will allow the system to transition from low stiffness to

extremely high stiffness when activating the solenoid valve, thus increasing the possible range of pressures and forces.

Acknowledgement

This research is part of the project PNRR-NGEU which has received funding from the MUR – DM 117/2023.

References

[1] Tawk, C., in het Panhuis, M., Spinks, G.M., Alici, G. (2019). Soft Pneumatic Sensing Chambers for Generic and Interactive Human–Machine Interfaces. *Advanced Intelligent Systems 1*, 1900002, https://doi.org/10.1002/aisy.201900002

[2] Yoshikawa, T. (2010). Multifingered robot hands: Control for grasping and manipulation. *Annual Reviews in Control*, vol. 34, no. 2, pp. 199-208, https://doi.org/10.1016/j.arcontrol.2010.09.001

[3] Shintake, J., Cacucciolo, V., Floreano, D., Shea, H. (2018). Soft Robotic Grippers. *Advanced Materials*, 30, 1707035, https://doi.org/10.1002/adma.201707035

[4] Stabile, C. J. , Levine, D. J., Iyer, G. M., Majidi, C., Turner, K. T. (2022). The Role of Stiffness in Versatile Robotic Grasping. *IEEE Robotics and Automation Letters*, vol. 7, no. 2, pp. 4733-4740, https://doi.org/10.1109/LRA.2022.3149036

[5] Jentoft, L. P., Wan, Q., Howe, R. D. (2014). Limits to compliance and the role of tactile sensing in grasping. *2014 IEEE International Conference on Robotics and Automation (ICRA)*, pp. 6394-6399, https://doi.org/10.1109/ICRA.2014.6907803

[6] Colucci, G., Visconte, C., Quaglia, G. (2023). Functional Design and Prototyping of a Novel Soft Fingertip with Variable Stiffness. In *Proceedings of I4SDG Workshop 2023. I4SDG 2023. Mechanisms and Machine Science*, vol. 134, https://doi.org/10.1007/978-3-031-32439-0_32

[7] Duretto, S., Colucci, G., Botta, A., Tagliavini, L., Jabari, M., Baglieri, L., Toccaceli, L., Amodio, F., Quaglia, G. (2025). Soft Pneumatic Sensing Chambers for Robotic Grasping. In *Advances in Service and Industrial Robotics. RAAD 2025. Mechanisms and Machine Science*, vol 190, https://doi.org/10.1007/978-3-032-02106-9_19

[8] Yuan, J., Liu, X., Xia, H., Huang, Y. (2021). Analytical solutions for inflation of pre-stretched elastomeric circular membranes under uniform pressure. *Theoretical and Applied Mechanics Letters*, vol. 11, no. 3, https://doi.org/10.1016/j.taml.2021.100243

[9] Xavier, M.S., Tawk, C.D., Yong, Y.K., Fleming, A.J. (2021). 3D-printed omnidirectional soft pneumatic actuators: Design, modeling and characterization. *Sensors and Actuators A: Physical* 332, 113199, https://doi.org/10.1016/j.sna.2021.113199

[10] Marechal, L., Balland, P., Lindenroth, L., Petrou, F., Kontovounisios, C., Bello, F. (2021). Towards a Common Framework and Database of Materials for Soft Robotics. *Soft Robotics*, vol. 8, no. 3, pp. 284-297, https://doi.org/10.1089/soro.2019.0115

[11] Duretto, S., Colucci, G., Tagliavini, L., Botta, A., Quaglia, G. (2026). Variable Stiffness Soft Pneumatic Sensing Chambers for Tactile Sensing and Haptic Devices. Preprint available at SSRN: http://dx.doi.org/10.2139/ssrn.6206763